arXiv:1805.05198v1 [quant-ph] 14 May 2018

Dynamics of an off-resonantly pumped superconducting qubit in a cavity

Raphaël Lescanne,[1,2,*] Lucas Verney,[2,1] Quentin Ficheux,[1,3] Michel H. Devoret,[4] Benjamin Huard,[3] Mazyar Mirrahimi,[2,5] and Zaki Leghtas[6,1,2,†]

[1] *Laboratoire Pierre Aigrain, Ecole Normale Supérieure, PSL Research University, CNRS, Université Pierre et Marie Curie, Sorbonne Universités, Université Paris Diderot, Sorbonne Paris-Cité, 24 rue Lhomond, 75231 Paris Cedex 05, France*

[2] *QUANTIC team, INRIA de Paris, 2 Rue Simone Iff, 75012 Paris, France*

[3] *Laboratoire de Physique, Ecole Normale Supérieure de Lyon, 46 allée d'Italie, 69364 Lyon Cedex 7, France*

[4] *Department of Applied Physics, Yale University, 15 Prospect St., New Haven, CT 06520, USA*

[5] *Yale Quantum Institute, Yale University, 17 Hillhouse Av., New Haven, CT 06520, USA*

[6] *Centre Automatique et Systèmes, Mines-ParisTech, PSL Research University, 60, bd Saint-Michel, 75006 Paris, France*

(Dated: May 15, 2018)

Strong microwave drives, referred to as pumps, are widely applied to superconducting circuits incorporating Josephson junctions in order to induce couplings between electromagnetic modes. This offers a variety of applications, from quantum-limited amplification, to quantum state and manifold stabilization. These couplings scale with the pump power, therefore, seeking strong couplings requires a detailed understanding of the behavior of such circuits in the presence of strong pumps. In this work, we probe the dynamics of a transmon qubit in a 3D cavity, for various pump powers and frequencies. For all pump frequencies, we find a critical pump power above which the transmon is driven into highly excited states, beyond the first seven states which we individually resolve through cavity spectroscopy. This observation is compatible with our theory describing the escape of the transmon state out of its Josephson potential well, into states resembling those of a free particle which does not induce any non-linear couplings.

Superconducting circuits are one of the leading platforms to implement quantum technologies. They host highly coherent electromagnetic modes whose parameters are engineered to fulfill a particular function. Josephson junctions (JJ) mediate non linear couplings between the circuit modes which can be arranged in a variety of topologies. By tailoring the type and strength of coupling, one can perform a multitude of tasks, such as amplifying signals [1–3], generating non-classical light [4, 5], stabilizing single quantum states [6, 7] or manifolds [8], releasing and catching propagating modes [9, 10], and simulating quantum systems [11]. The full in-situ control of the couplings mediated by the Josephson nonlinearity necessitates a key ingredient: a strong coherent microwave drive, referred to as a pump. Typically, the pump frequency is not resonant with any mode and instead verifies a specific frequency matching condition in order to select the desired coupling (so-called parametric pumping). In the low pump power regime, the coupling strength increases with the pump power. Couplings much stronger than internal dissipation rates are instrumental for high fidelity quantum state preparation, or to increase the efficacy of quantum error correction protocols based on quantum manifold stabilization with parametric pumping [12]. Seeking strong couplings poses the question: what is the behavior of a Josephson circuit in the presence of a strong off-resonant pump? Answering this question will reveal the limits of current designs and guide us towards circuits better suited to parametric pumping.

Theoretical models have been proposed to solve the dynamics of a superconducting circuit in the presence of many photons [13–16] in the context of high fidelity single-shot qubit readout [17]. The measurements carried out on our device are incompatible with those models, and motivate a more general treatment to account for strong off-resonant pumps in superconducting circuits [18].

Our device consists of a single transmon [19] in a 3D copper cavity [20] coupled to a transmission line. The system is well modeled by the circuit depicted in Fig. 1a, whose Hamiltonian is given by [19]

$$\boldsymbol{H}(t) = 4E_C\boldsymbol{N}^2 - E_J\cos(\boldsymbol{\theta}) + \hbar\omega_a\boldsymbol{a}^\dagger\boldsymbol{a} + \hbar g\boldsymbol{N}\left(\boldsymbol{a}+\boldsymbol{a}^\dagger\right) + \hbar\mathcal{A}_p(t)\left(\boldsymbol{a}+\boldsymbol{a}^\dagger\right), \quad (1)$$

where $\boldsymbol{N}$ is the number operator for the Cooper pairs which were transfered across the junction. A fluctuating charge bias across the junction can be modeled by shifting $\boldsymbol{N}$ by the gate charge number $N_g(t)$. The operator $\boldsymbol{N}$ has integer eigenvalues and hence the phase degree of freedom θ is defined over the bounded set $[-\pi,\pi[$ with periodic boundary conditions [21]. The operator $\cos(\boldsymbol{\theta})$ is the transfer operator for Cooper pairs across the junction while $\boldsymbol{a}^\dagger$ and $\boldsymbol{a}$ are the creation and annihilation operators for the resonator mode. Here, E_C is the charging energy of the superconducting island (within the dashed lines in Fig. 1a), E_J is the Josephson energy, ω_a is the angular frequency of the resonator in the absence of the JJ (E_J taken to be 0) which is known as the bare resonator frequency and g is the coupling rate between the trans-

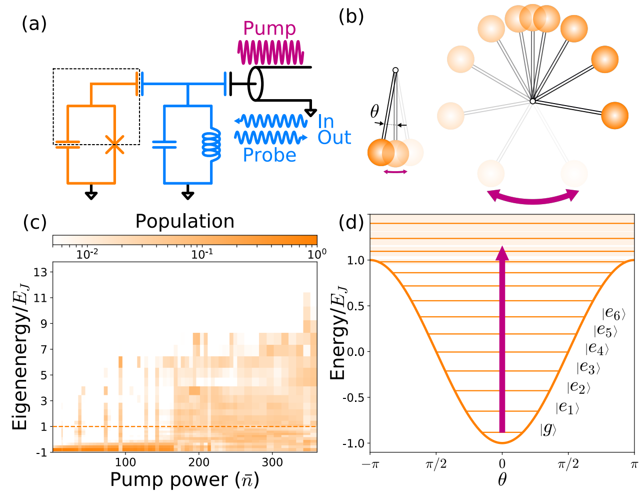

FIG. 1. Principle of the experiment demonstrating the effect of a strong pump on a Josephson circuit. (**a**) A superconducting island (within the dashed lines) is coupled to ground through a Josephson junction (JJ), which is shunted by a capacitor, forming a transmon mode (orange). It is capacitively coupled to an LC resonator (blue) which represents the lowest mode of a 3D waveguide cavity. The system is pumped and probed through a transmission line (black). (**b**) Classical picture: The transmon is represented by a pendulum [19], where the deviation angle from equilibrium, denoted θ, is the phase difference across the JJ. The gravitational potential energy represents the Josephson energy. For small pump powers (left), the pendulum acquires a small kinetic energy and oscillates around its equilibrium. For large pump powers (right), it acquires sufficient energy to escape from its trapping potential well, and rotates indefinitely. (**c**) Numerical simulation of the population (color) of the energy levels of the transmon (y-axis) as a function of the number of photons $\bar{n}$ [23] in the resonator due to the pump (x-axis). For small $\bar{n}$, the transmon is close to its ground state, except for small population bursts (see text). Above a critical $\bar{n}$ (which is about 170 photons for our system parameters), the transmon jumps into highly excited states above its cosine potential (orange dashed line). (**d**) Quantum picture: cosine potential and energy levels (orange lines) for charge offset $N_g = 0$. Pink areas represent the band of levels appearing when varying N_g [24]. Large pump powers (big arrow) induce transitions from the ground state $|g\rangle$ with a phase localized around $\theta = 0$, into highly excited states with a delocalized phase.

mon and the resonator. Note that this definition of g differs from the one usually used in the Jaynes-Cummings Hamiltonian [22]. The pump couples capacitively to the circuit, and is accounted for by the second line in (1), where $\mathcal{A}_p(t) = A_p \cos(\omega_p t)$, A_p and ω_p being the pump amplitude and angular frequency. Our pump frequencies are in the vicinity of the resonator frequency, therefore, we neglect the direct coupling of the pump to the transmon. Moreover, this coupling can be taken into account by redefining A_p [18]. The transmon mode has an infinite number of energy levels, and the two lowest ones are usually used as a qubit.

Our physical picture of the dynamics of a pumped transmon in a cavity is the following. When the pump power is sufficiently large, the transmon is excited above its bounded potential well (Fig. 1c,d). This is analogous to an electron escaping from the bound states of the atomic Coulomb potential and leaving the atom ionized. The transmon can occupy highly excited states which resemble charge states, or equivalently, plane waves in the phase representation. A classical analogy would be a strongly driven pendulum which rotates indefinitely, making turns around its anchoring point (Fig. 1b). When occupying such a state, the transmon behaves like a free particle which is almost not affected by the cosine potential. Thus the Josephson energy can be set to zero in Eq. (1). The Hamiltonian is now that of a superconducting island capacitively coupled to a resonator, with no Josephson junction. The island-resonator coupling term commutes with the Hamiltonian of the island, which consists of the charging energy only. The coupling is now longitudinal and therefore the cavity frequency is fixed to the bare frequency ω_a, independently of the island state.

The dynamics governed by Hamiltonian (1) is difficult to numerically simulate in the regime of large pump amplitudes for two reasons. First, the simulated Hilbert space needs to be large. Indeed, the number of transmon states needs to be much larger than the number of states in the well. For our experimental parameters we find that about 45 states are sufficient. Moreover, the resonator is driven to large photon numbers and thus also occupies many states. Second, the pump amplitude is so large that we reach regimes where $A_p \gg \omega_a$. It is therefore excluded to use the rotating wave approximation in its usual form. These two difficulties are surmounted by the theory introduced in [18]. Using an adequate change of frame in which the resonator is close to the vacuum, we can decrease the number of computed states to 10 for the resonator, hence reducing the dimensionality of the Hilbert space [23]. Since $\boldsymbol{H}(t)$ is $2\pi\omega_p^{-1}$-periodic, we use Floquet-Markov theory [25, 26], to find the system steady state, as shown in Fig. 1c. This theory assumes weak coupling to the bath, but can treat pumps of arbitrary amplitude and frequency. For small pump powers, the transmon remains close to its ground state, and after the power is increased beyond a critical value, it is driven into highly excited states, above its cosine potential (orange dashed line in Fig. 1c). For this simulation, we take $N_g = 0$ and find that other values of N_g lead to the same qualitative behavior [18].

The parameters of Hamiltonian (1) are deduced from measurements involving a low number of excitations in the system. In this regime, it is well approximated by the Hamiltonian of two non-linearly coupled effective modes, one transmon qubit-like and one resonator-like, respectively denoted by subscripts q and r [27]:

$$\begin{aligned}\boldsymbol{H}_{\rm low}(t)/\hbar = &\ \bar{\omega}_q \boldsymbol{a}_q^\dagger \boldsymbol{a}_q - \frac{\alpha_q}{2}\left(\boldsymbol{a}_q^\dagger\right)^2 \boldsymbol{a}_q{}^2 - \chi_{qr}\boldsymbol{a}_q^\dagger \boldsymbol{a}_q \boldsymbol{a}_r^\dagger \boldsymbol{a}_r \\ &+ \bar{\omega}_r \boldsymbol{a}_r^\dagger \boldsymbol{a}_r - \frac{\alpha_r}{2}\left(\boldsymbol{a}_r^\dagger\right)^2 \boldsymbol{a}_r{}^2 \\ &+ \mathscr{A}_{p,r}(t)\left(\boldsymbol{a}_r + \boldsymbol{a}_r^\dagger\right), \qquad (2)\end{aligned}$$

where $\bar{\omega}_{q,r}$ are the modes angular frequencies, $\alpha_{q,r}$ their Kerr non-linearities, and χ_{qr} their dispersive coupling. In this basis, the pump is represented by the term in $\mathscr{A}_{p,r}(t) = A_{p,r}\cos(\omega_p t)$, with a renormalized amplitude $A_{p,r}$, where we neglect the linear coupling of the pump to mode q.

We measure $\bar{\omega}_q/2\pi = 5.353$ GHz, $\bar{\omega}_r/2\pi = 7.761$ GHz, $\alpha_q/2\pi = 173$ MHz and $\chi_{qr}/2\pi = 5$ MHz. In order to compute E_J, E_C, g and ω_a, we write Hamiltonian (1) in matrix form in the charge basis for the transmon and the Fock basis for the resonator. We calculate the differences in energy of the lowest energy levels, which are directly related to the parameters of Hamiltonian (2). We fit the measured values with the following parameters: $E_C/h = 166$ MHz, $E_J/h = 23.3$ GHz, $g/2\pi = 179$ MHz and $\omega_a/2\pi = 7.739$ GHz. We also infer $\alpha_r/2\pi = 43$ kHz. The depth of the cosine potential is $2E_J$ and the level spacing is approximately $\sqrt{8E_J E_C}$ [19] hence, the number of confined levels is about 10, as shown in Fig. 1d.

We experimentally observe the transmon jump into highly excited states by performing the spectroscopy of the resonator while the pump is applied (Fig.2). For small pump powers, the system is well described by the low energy Hamiltonian (2). The pump populates the resonator with photons at the pump frequency with an average number $\bar{n}_r = \left|\frac{A_{p,r}/2}{i(\omega_r-\omega_p)+\kappa_r/2}\right|^2$, and shifts the resonance to $\omega_r(\bar{n}_r) = \bar{\omega}_r - 2\alpha_r\bar{n}_r$ [8, Supplement section 2.1]. We calibrate the photon number $\bar{n}_r$ [23, Section 2] and, using the anharmonicity α_r deduced from the model (2), we plot $\omega_r(\bar{n}_r)$ (solid line in Fig. 2b). The data points match this prediction in the regime of small photon numbers, over a wide range of pump frequencies. This linear dependence is disrupted by abrupt frequency jumps, as seen for a pump power of about $30P_{1ph}$ in Fig. 2a. This behavior suggests that the system frequencies, at this specific power, have shifted into resonance with a process which excites the transmon. This resembles the population bursts observed for example at 90 photons in the simulation of Fig. 1c, before the population jumps at around 170 photons.

Above a critical $\bar{n}_r$ (of about 100 photons for the most detuned pump frequencies), the resonance jumps to a new frequency close to $\omega_a/2\pi$ (arrow in Fig. 2b), which is independent of the pump frequency and power. This is the resonator frequency expected when the transmon is highly excited so that the JJ behaves as an "open". Such a jump of the resonance has been modeled in previous works with a strong probe close to resonance with

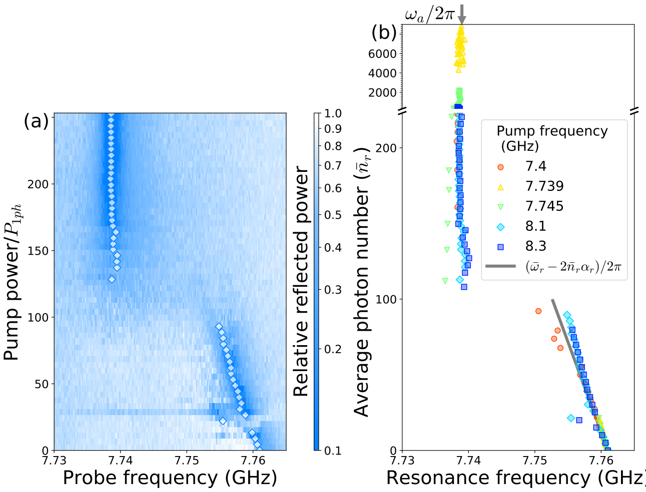

FIG. 2. Effect of the pump on the cavity resonance frequency. (**a**) Relative reflected power of a weak probe as a function of probe frequency (x-axis), and pump power (y-axis) in units of P_{1ph}, the power needed to populate the cavity with one photon in average. The pump frequency is fixed at 8.1 GHz, about 300 MHz above the cavity frequency. The reduced reflected power is due to internal losses when the probe is resonant with the cavity. We indicate the fitted cavity resonance $\omega_r/2\pi$ with white diamonds. As the pump power increases, two regimes are distinguishable. For small powers, ω_r shifts linearly with the pump power. Above a critical power, the cavity resonance jumps to a new frequency $\omega_a/2\pi = 7.739$ GHz which is independent of pump power. (**b**) Fitted cavity resonance as a function of pump power for various pump frequencies. Pump powers are converted into the mean number $\bar{n}_r$ of photons at the pump frequency inside the resonator [23, Section 2]. The y-axis of (a) and (b) slightly differ because $\bar{n}_r$ takes into account the resonator frequency shift. The general behavior is the same for all pump frequencies. The low power linear dependence is well reproduced by the AC Stark shift [8] for an independently measured Kerr α_r (solid gray line).

the resonator and in the absence of a pump. Those models involve a two-level [13, 14], multi-level [15] or Duffing [16] approximations for the transmon. In the following paragraphs, we show that such approximations are incompatible with our measurements. Instead, one needs to consider all levels confined in the cosine potential and a number of levels above which depends on the pump power.

For states well confined inside the cosine potential, the transmon state is encoded in the resonance frequency of the resonator. As seen from Hamiltonian (2), each additional excitation in the transmon pulls the resonator frequency to $\omega_r(n_q) = \bar{\omega}_r - n_q\chi_{qr}$ (Fig. 3a). However, for states above the cosine potential, the resonator adopts a frequency ω_a which is now independent of the particular transmon state.

The highly excited nature of the transmon can be confirmed by turning off the pump, and waiting for the transmon to decay to lower lying states which can be resolved

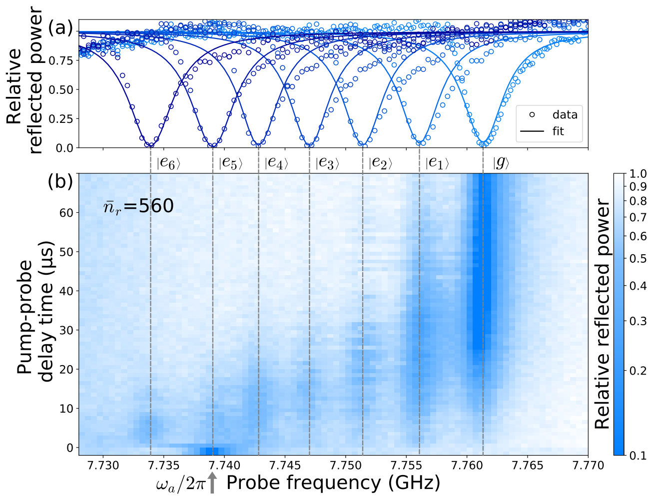

FIG. 3. Probing the transmon decay out of highly excited states populated by a strong off-resonant pump. (**a**) Cavity spectroscopy after the transmon is prepared in various eigenstates. Due to the dispersive coupling between the transmon and the cavity, the cavity frequency depends on the number of excitations k in the transmon. Each transmon state $|e_k\rangle$ (k =1 to 6) is prepared using a k-photon π-pulse [23, FigS2] and higher states could not be prepared due to charge noise [23, Section 4]. (**b**) Time resolved measurement: first, a pump is applied for 50 μs at 8.1 GHz populating the cavity with a sufficiently large photon number to induce a jump in ω_r, here $\bar{n}_r = 560$. After a time-delay t, a weak probe is applied for 2 μs. We plot the relative reflected power of the probe as a function of probe frequency (x-axis), and time-delay t (y-axis). For $t < 0$, as in Fig. 2, the cavity is probed while the pump is on, and the resonance frequency is $\omega_a/2\pi$, confirming that the system has jumped. At $t > 0$, the photons in the cavity rapidly decay at a rate $\kappa_r = 1/(55\text{ ns})$, and the cavity can now be used, as in Fig. 3a, to read the transmon state. The transmon is found in a highly excited state, and after $t = 60$ μs, it has fully decayed into its ground state which is compatible with $T_1 = 14$ μs.

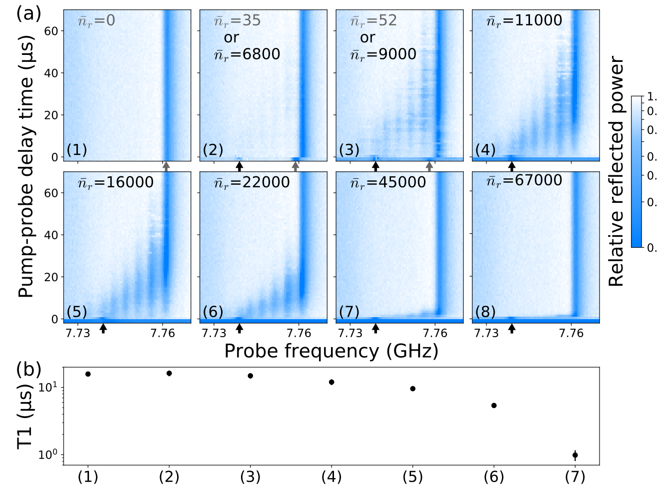

FIG. 4. Transmon relaxation following a pump pulse of increasing power. (**a**) Same experiment as in Fig. 3b with increasing pump power (a1 to a8). The pump frequency is fixed at $f_p = \omega_a/2\pi = 7.739$ GHz in order to populate the cavity with a large number of photons. Each pump power is converted into the mean number of photons $\bar{n}_r$ in the cavity. The conversion factor depends on the observed cavity frequency at $t \leq 0$, indicated by the arrows (see [23, Section 2]). (**a1**) The pump power is too low to induce a shift or a jump in the cavity frequency. (**a2**-**a3**) At intermediate pump powers, the system is in a statistical mixture of two configurations, as indicated by the two arrows at $t < 0$. First, a weakly shifted resonance due to the AC Stark shift with a small cavity population. Second, a resonance at ω_a coinciding with the pump frequency and hence a large cavity population. (**a4**-**a5**) At higher pump powers, the cavity frequency always jumps to ω_a and the transmon decays as in Fig. 3b. (**a6**-**a8**) At even higher pump powers, the transmon decay rate increases significantly. (**b**) Transmon T_1 (y-axis) measured 50 μs after a pump is applied. The pump duration and powers (x-axis) correspond to the ones used for the experiments shown in (a). We observe a decrease in T_1 as the pump power increases, which is consistent with an increasing quasi-particle density induced by the pump [28, 29], and explains the significantly higher decay rates in (a6-a8). For pump powers (1-3), T_1 is marginally reduced, while the system dynamics is highly affected (a1-a3). The T_1 corresponding to (a8) was too small to be accurately measured.

by probing the resonator frequency. In this experiment, the highest of these states was the sixth excited state $|e_6\rangle$. As expected, after the pump is turned off ($t = 0$ in Fig. 3b), we observe a population decay of the transmon compatible with a highly excited state at $t \leq 0$. It is interesting to observe that $\omega_r(n_q = 5) \approx \omega_a$ and $\omega_r(n_q = 6) < \omega_a$.

Strongly pumping a superconducting circuit generates non-equilibrium quasiparticles [28, 29], which poses the question: what is the influence of quasiparticles on this dynamics? We detect whether quasiparticles have been generated by the pump pulse by measuring the transmon T_1 after a time delay large enough to ensure that all modes have decayed back to their ground states. We find that for the pump frequency and power used for the experiment of Fig. 3b, the T_1 is unaffected [23]. This indicates that the pump can expel the transmon out of its potential well, without generating a measurable amount of quasiparticles, and therefore the simulation of Fig. 1c, which does not include quasiparticles, is relevant.

In order to observe a measurable decrease in T_1, we need to insert a much larger number of photons in the resonator. We enter this regime by applying a pump at frequency ω_a, so that the pump is resonant with the resonator at large powers. As shown in Fig. 4b, the T_1 drops at high pump powers indicating that we have successfully generated quasiparticles. Furthermore, we find that the transmon T_1 recovers its nominal value of $T_1 = 15$ μs after a few milliseconds, a typical timescale for quasiparticle recombination [28, 29]. In Fig. 4a, we probe the transmon dynamics as in Fig. 3b, in the presence of pump-induced quasiparticles. The increased quasiparticle density does not qualitatively modify the transmon dynamics, but only increases the decay rate back to its ground state.

In conclusion, we have measured the dynamics of a transmon in a 3D cavity in the presence of a strong off-resonant pump. Despite large detunings between the pump and all mode frequencies, the transmon is driven into highly excited states. Our measurements are in qualitative agreement with our theory describing the transmon escaping out of its potential well. The transmon then behaves like a free-particle which no longer induces any non-linear couplings. This escape, which is due to the boundedness of the cosine potential, could be prevented by adding an unbounded parabolic potential, provided by an inductive shunt. One could then further increase the non-linear couplings by increasing the pump power, without driving the transmon into free particle states and losing the resource of non-linearity. Our research points towards inductively shunted JJs as better suited than standard transmons for pump-induced non-linear couplings [18].

Acknowledgments The authors thank Pierre Rouchon and Takis Kontos for fruitful discussions and Matthieu Dartiailh for developing the instrument control software [30]. This work was supported by the ANR grant ENDURANCE, and the EMERGENCES grant ENDURANCE of Ville de Paris. The devices were fabricated within the consortium Salle Blanche Paris Centre. MHD acknowledges ARO support.

* raphael.lescanne@lpa.ens.fr
† zaki.leghtas@mines-paristech.fr

[1] M. A. Castellanos-Beltran, K. D. Irwin, G. C. Hilton, L. R. Vale, and K. W. Lehnert, Nature Physics **4**, 929 (2008).
[2] N. Bergeal, F. Schackert, M. Metcalfe, R. Vijay, V. E. Manucharyan, L. Frunzio, D. E. Prober, R. J. Schoelkopf, S. M. Girvin, and M. H. Devoret, Nature **465**, 64 (2010).
[3] C. Macklin, K. O'Brien, D. Hover, M. E. Schwartz, V. Bolkhovsky, X. Zhang, W. D. Oliver, and I. Siddiqi, Science **350**, 307 (2015).
[4] M. Pechal, L. Huthmacher, C. Eichler, S. Zeytinoğlu, A. A. Abdumalikov, S. Berger, A. Wallraff, and S. Filipp, Phys. Rev. X **4**, 041010 (2014).
[5] E. Flurin, N. Roch, F. Mallet, M. H. Devoret, and B. Huard, Physical Review Letters **109**, 183901 (2012).
[6] K. W. Murch, U. Vool, D. Zhou, S. J. Weber, S. M. Girvin, and I. Siddiqi, Phys. Rev. Lett. **109**, 183602 (2012).
[7] S. Shankar, M. Hatridge, Z. Leghtas, K. M. Sliwa, A. Narla, U. Vool, S. M. Girvin, L. Frunzio, M. Mirrahimi, and M. H. Devoret, Nature **504**, 419 (2013).
[8] Z. Leghtas, S. Touzard, I. M. Pop, A. Kou, B. Vlastakis, A. Petrenko, K. M. Sliwa, A. Narla, S. Shankar, M. J. Hatridge, M. Reagor, L. Frunzio, R. J. Schoelkopf, M. Mirrahimi, and M. H. Devoret, Science **347**, 853 (2015).
[9] A. Narla, S. Shankar, M. Hatridge, Z. Leghtas, K. M. Sliwa, E. Zalys-Geller, S. O. Mundhada, W. Pfaff, L. Frunzio, R. J. Schoelkopf, and M. H. Devoret, Phys. Rev. X **6**, 031036 (2016).
[10] W. Pfaff, C. J. Axline, L. D. Burkhart, U. Vool, P. Reinhold, L. Frunzio, L. Jiang, M. H. Devoret, and R. J. Schoelkopf, Nature Physics **13**, 882 EP (2017).
[11] S. Puri, C. K. Andersen, A. L. Grimsmo, and A. Blais, Nature Communications **8**, 15785 EP (2017).
[12] M. Mirrahimi, Z. Leghtas, V. V. Albert, S. Touzard, R. J. Schoelkopf, L. Jiang, and M. H. Devoret, New J. Phys. **16**, 045014 (2014).
[13] T. K. Mavrogordatos, G. Tancredi, M. Elliott, M. J. Peterer, A. Patterson, J. Rahamim, P. J. Leek, E. Ginossar, and M. H. Szymańska, Phys. Rev. Lett. **118**, 040402 (2017).
[14] M. Boissonneault, J. M. Gambetta, and A. Blais, Phys. Rev. Lett. **105**, 100504 (2010).
[15] L. S. Bishop, E. Ginossar, and S. M. Girvin, Phys. Rev. Lett. **105**, 100505 (2010).
[16] M. Elliott and E. Ginossar, Phys. Rev. A **94**, 043840 (2016).
[17] M. D. Reed, L. DiCarlo, B. R. Johnson, L. Sun, D. I. Schuster, L. Frunzio, and R. J. Schoelkopf, Phys. Rev. Lett. **105**, 173601 (2010).
[18] L. Verney, R. Lescanne, M. H. Devoret, Z. Leghtas, and M. Mirrahimi, In preparation (2018).
[19] J. Koch, T. M. Yu, J. Gambetta, A. A. Houck, D. I. Schuster, J. Majer, A. Blais, M. H. Devoret, S. M. Girvin, and R. J. Schoelkopf, Phys. Rev. A **76**, 042319 (2007).
[20] H. Paik, D. I. Schuster, L. S. Bishop, G. Kirchmair, G. Catelani, A. P. Sears, B. R. Johnson, M. J. Reagor, L. Frunzio, L. I. Glazman, S. M. Girvin, M. H. Devoret, and R. J. Schoelkopf, Phys. Rev. Lett. **107**, 240501 (2011).
[21] S. Girvin, Les Houches Session XCVI, Quantum machines , 113 (2011).
[22] A. Wallraff, D. I. Schuster, A. Blais, L. Frunzio, R. S. Huang, J. Majer, S. Kumar, S. M. Girvin, and R. J. Schoelkopf, Nature **431**, 162 (2004).
[23] See supplemental material for details.
[24] A. Cottet, Theses, Université Pierre et Marie Curie - Paris VI (2002).
[25] M. Grifoni and P. Hänggi, Physics Reports **304**, 229 (1998).
[26] J. Johansson, P. Nation, and F. Nori, Computer Physics Communications **184**, 1234 (2013).
[27] S. E. Nigg, H. Paik, B. Vlastakis, G. Kirchmair, S. Shankar, L. Frunzio, M. H. Devoret, R. J. Schoelkopf, and S. M. Girvin, Phys. Rev. Lett. **108**, 240502 (2012).
[28] C. Wang, Y. Y. Gao, I. M. Pop, U. Vool, C. Axline, T. Brecht, R. W. Heeres, L. Frunzio, M. H. Devoret, G. Catelani, L. I. Glazman, and R. J. Schoelkopf, Nature Communications **5**, 5836 EP (2014).
[29] U. Vool, I. M. Pop, K. Sliwa, B. Abdo, C. Wang, T. Brecht, Y. Y. Gao, S. Shankar, M. Hatridge, G. Catelani, M. Mirrahimi, L. Frunzio, R. J. Schoelkopf, L. I. Glazman, and M. H. Devoret, Phys. Rev. Lett. **113**, 247001 (2014).
[30] Https://github.com/Exopy.

Supplemental material for "Dynamics of an off-resonantly pumped superconducting qubit in a cavity"

SAMPLE FABRICATION

The sample measured in this work is the same one as in [S1]. The transmon is made of a single aluminum Josephson junction and is embedded in a copper cavity of $26.5 \times 26.5 \times 9.5$ mm^3 thermalized on the base plate of a dilution fridge at about 10 mK. More details can be found in [S1, Sections 1.A and 1.B].

PHOTON NUMBER CALIBRATION

In this section, we explain how we convert a pump power in mW, to an average number of photons at the pump frequency inside the cavity. We exploit the AC Stark shift and measurement induced-dephasing [S2], where a drive on the resonator inserts photons which detune and dephase the qubit. We use a 2-level approximation of the low energy Hamiltonian (Eq. (2) in the main text):

$$\boldsymbol{H}^{(2)}_{\mathrm{low}}/\hbar = \omega_q \frac{\boldsymbol{\sigma}_z}{2} + \omega_r \boldsymbol{a}_r^\dagger \boldsymbol{a}_r - \chi_{qr} |e\rangle\langle e| \boldsymbol{a}_r^\dagger \boldsymbol{a}_r + A_{p,r}\cos(\omega_p t)\left(\boldsymbol{a}_r + \boldsymbol{a}_r^\dagger\right) \tag{S1}$$

where $\sigma_z = |e\rangle\langle e| - |g\rangle\langle g|$, and $|g\rangle, |e\rangle$ are the transmon's ground and first excited states. Moving into a frame rotating at the pump frequency ω_p for the resonator, and the qubit frequency ω_q for the qubit, and performing the rotating wave approximation (RWA), we get

$$\bar{\boldsymbol{H}}^{(2)}_{\mathrm{low}}/\hbar = \Delta \boldsymbol{a}_r^\dagger \boldsymbol{a}_r - \chi_{qr} |e\rangle\langle e| \boldsymbol{a}_r^\dagger \boldsymbol{a}_r + A_{p,r}\boldsymbol{a}_r/2 + A_{p,r}\boldsymbol{a}_r^\dagger/2 \ ,$$

where $\Delta = \omega_r - \omega_p$.

Depending on the qubit state $|g\rangle$ [resp: $|e\rangle$], the resonator reaches a steady state which is a coherent state of amplitude α_g [resp: α_e], where:

$$\alpha_g = \frac{-iA_{p,r}/2}{i\Delta + \kappa_r/2}$$
$$\alpha_e = \frac{-iA_{p,r}/2}{i(\Delta - \chi_{qr}) + \kappa_r/2} \ .$$

The measurement induced complex detuning is [S2]

$$\delta_m = -\chi_{qr}\alpha_e\alpha_g^* = -\chi_{qr}\frac{A_{p,r}^2/4}{\left(i(\Delta - \chi_{qr}) + \kappa_r/2\right)\left(-i\Delta + \kappa_r/2\right)} \ ,$$

Re(δ_m) being the AC Stark frequency shift, and -Im(δ_m) being the measurement induced dephasing rate. The quantity $A_{p,r}^2$ is proportional to the output power of our instrument P_p, and hence we write it in the following form: $A_{p,r}^2 = \kappa_r^2 C P_p$, where C is the proportionality constant we aim to calibrate and is expressed in a number of photons per mW. Since our microwave input lines do not have a perfectly flat transmission over a GHz range, C can be dependent on ω_p. We get:

$$\delta_m(\omega_p, P_p) = -C\frac{\kappa_r^2\chi_{qr}P_p/4}{\left(i(\Delta - \chi_{qr}) + \kappa_r/2\right)\left(-i\Delta + \kappa_r/2\right)} \ . \tag{S2}$$

For each pump frequency ω_p, we vary the pump power P_p between 0 and $P_{p,max}$, and perform a T_2 Ramsey experiment. The Ramsey fringes oscillation frequency and exponential decay provide a complex frequency shift δ_{tot}, such that Re(δ_{tot}) is the oscillation frequency, and -Im(δ_{tot}) is the dephasing rate. We have

$$\delta_{\mathrm{tot}}(\omega_p, P_p) = \delta_0 + \delta_m(\omega_p, P_p) \ , \tag{S3}$$

where δ_0 is due to the chosen drive-qubit detuning and to the qubit dephasing rate in the absence of the pump. Thus, we measure δ_{tot}, and the only unknown is the constant C, which we fit at each pump frequency. In Fig. S1, we plot for each pump frequency, δ_{tot} (open circles), and the fitted values (crosses), where C is the only fitting parameter. Once we know C, the average photon number is given by

$$\bar{n}_r(\omega_p, P_p) = \left|\frac{-iA_{p,r}/2}{i(\omega_r - \omega_p) + \kappa_r/2}\right|^2 \tag{S4}$$
$$= CP_p\frac{\kappa_r^2/4}{(\omega_r - \omega_p)^2 + \kappa_r^2/4} \ , \tag{S5}$$

where ω_r is the measured resonance frequency which itself depends on ω_p and P_p. We use Eq. (S7) to calculate all the given values of $\bar{n}_r$, and for the y-axis of Fig. 2b in the main text.

MULTI-PHOTON QUBIT DRIVE

In the main paper, we show that at large pump powers, when the resonator frequency jumps, the transmon is in a highly excited state. We observe the decay of the transmon to its ground state (Fig. 3b of the main text), and verify that the measured resonances coincide with the resonator frequency when the transmon is prepared in excited state $|e_k\rangle$ (Fig. 3a of the main text). In order to drive the transmon from its ground state into state $|e_k\rangle$, we apply a strong pulse at frequency ω_{0k}/k where

$$\omega_{0k} = \frac{E_k - E_0}{\hbar} \ . \tag{S6}$$

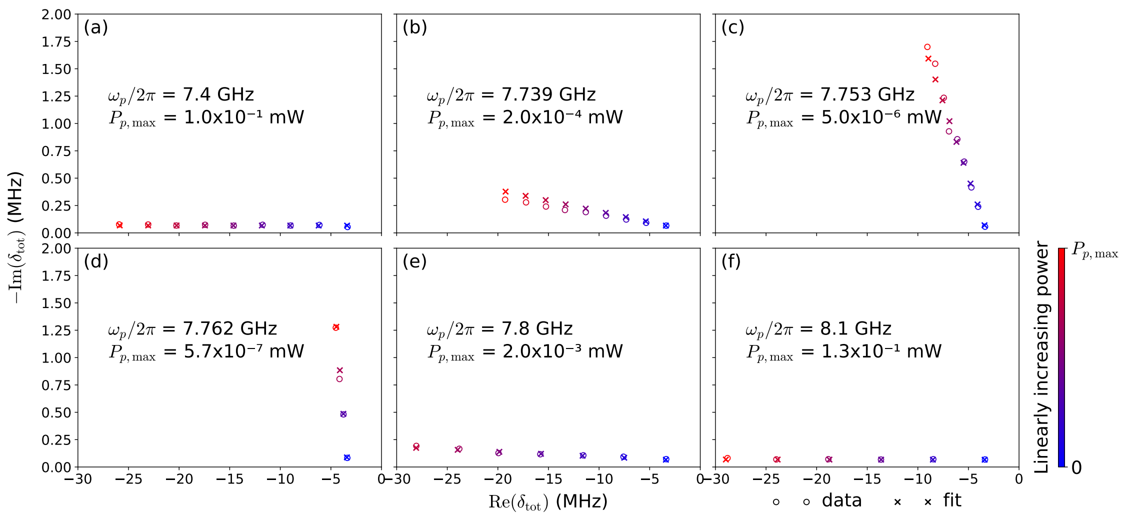

FIG. S1. Calibration to convert the pump power (mW) into an average number of photons $\bar{n}_r$, using the AC Stark shift and measurement-induced dephasing [S2]. By performing a Ramsey experiment in the presence of a pump at frequency ω_p and power P_p, we measure the detuning between the drive and the qubit $\delta_q(\omega_p, P_p)$, and the qubit dephasing rate $\gamma_\phi(\omega_p, P_p)$. We introduce $\delta_{tot} = \delta_q - i\gamma_\phi$. For each plot (a) to (f), the pump frequency is fixed, and γ_{tot} is plotted in the complex plane (hollow circles), for increasing P_p (blue is 0 mW, red is $P_{p,\max}$). For each pump frequency, the data points are fitted with Eq. (S3), where δ_m is given in Eq. (S2), and the constant C is the only fitting parameter. All other parameters: $\Delta, \kappa_r, \chi_{qr}, P_p, \delta_0$ are measured independently. (a),(f) Large detuning between the pump and the cavity. The pump mostly induces a detuning on the qubit, without inducing any dephasing. (d) The pump is resonant with the cavity, and mostly induces dephasing on the qubit. (b), (c), (e) Intermediate regimes where the pump both dephases and detunes the qubit.

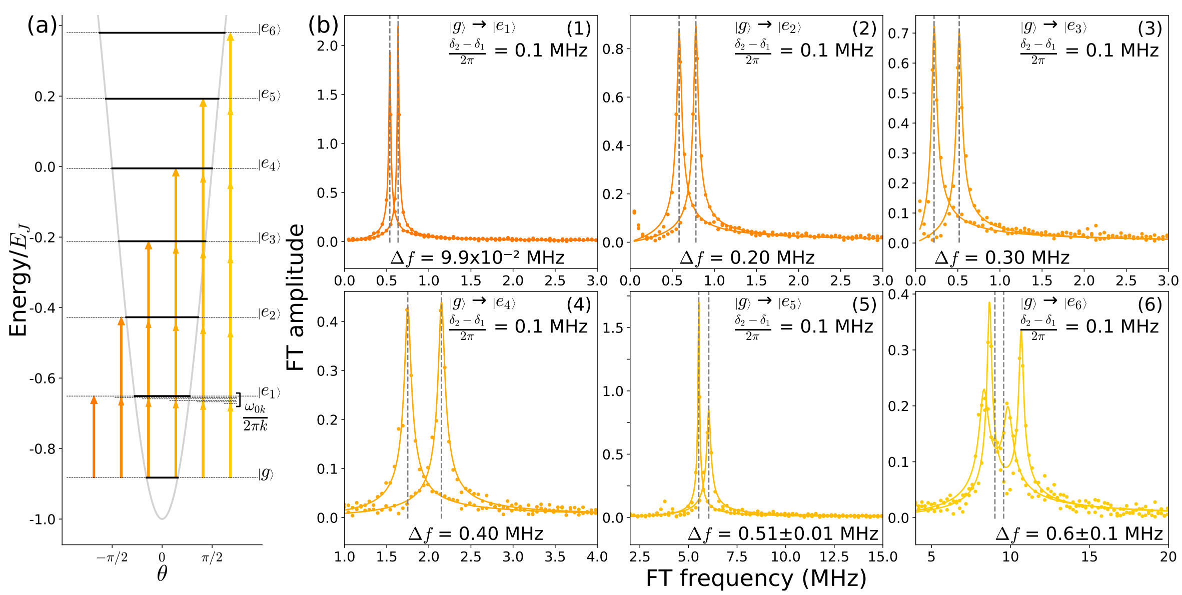

FIG. S2. Characterization of $k-$photon transitions. (a) Bottom of the cosine potential well of the transmon (grey line) in units of E_J (y-axis), as a function of the phase across the junction (x-axis). The ground state $|g\rangle$ and the first six excited states $|e_{k=1\ldots6}\rangle$ are represented (black horizontal lines). Each excited state $|e_k\rangle$ is prepared with a k-photon transition (arrows) with a drive at $\omega_d = \omega_{0k}/k$ (see text). (b1)-(b6) Fourier transform (FT) of a Ramsey signal (dots) for two different drive detunings δ_1 and $\delta_2 = \delta_1 + 2\pi \times 0.1$ MHz. The data is fitted (line) by the Fourier transform of an exponentially decaying cosine function (a sum of two cosines is needed for (b6)), which provides the detuning between the k-photon drive with effective frequency $k\omega_d$ and the transition frequency ω_{0k}. We verify that the difference between these detunings Δ_f scales as $k\left(\delta_2 - \delta_1\right)/2\pi$, as expected for a $k-$photon transition. Unlike (b1)-(b5), in (b6) we observe two peaks for each curve. This shows that the Ramsey signal has two frequency components, which is a consequence of quasi-particles tunneling across the junction (see text and Fig.S3).

E_k is the eigenenergy of eigenstate $|e_k\rangle$, and E_0 is the eigenenergy of the ground state $|g\rangle$. This induces a k-photon transition between $|g\rangle$ and $|e_k\rangle$, as schematically represented in Fig. S2b. This $k-$photon transition is then used to perform all standard qubit experiments, such as Rabi oscillations between $|g\rangle$ and $|e_k\rangle$, T_2 Ramsey and T_1 measurements. We verify that this is indeed a k-photon transition by performing a Ramsey measurement: two $\pi/2$ rotations with a drive at frequency ω_d slightly detuned from ω_{0k}/k, separated by a varying time, and followed by the measurement of σ_z. We obtain the oscillation frequency of the Ramsey fringes by taking the Fourier transform of the measurement (Fig. S2). If we detune the drive frequency by δ: $\omega_d = \omega_{0k}/k - \delta$, then $k\omega_d$ is detuned from the resonance ω_{0k} by $k\delta$. We perform a first Ramsey experiment with a drive detuned by δ_1, which serves as a reference. A second Ramsey experiment is performed with a detuning $\delta_2 = \delta_1 + 2\pi \times 0.1$ MHz. By subtracting the frequencies of the Ramsey fringes, denoted Δ_f, we get $\Delta_f = k\left(\delta_2 - \delta_1\right)/2\pi$, as shown in Fig. S2b1-b6.

CHARGE NOISE

Observing Fig. S2b6, we see that the Ramsey signal is not composed of a single frequency. This is reminiscent of charge noise, where a single quasiparticle is tunneling across the junction in and out of the superconducting island, thus changing its charge parity. This parity change corresponds to changes between N_g and $N_g \pm 1/2$, which occur on the millisecond timescale [S3]. Our Ramsey measurements take 16 seconds, hence our data shows the average of these charge offset configurations. Note that despite the fact that we are deep in the transmon regime: $E_J/E_C = 140$, the higher energy levels disperse with charge offset.

We confirm this effect by plotting the Fourier transform of the Ramsey signal for the $|g\rangle$ to $|e_6\rangle$ transition vs. time (Fig. S3). We see the slow symmetric drift of the two frequencies, due to the background charge motion [S3].

The following energy level ($|e_7\rangle$ and above) fluctuate much more than $|e_6\rangle$ with charge offsets, and this is why we could not prepare the transmon in states above $|e_6\rangle$.

NUMERICAL SIMULATION

In this section, we describe the numerical simulation of Fig. 1c of the main text. The details of this simulation can be found in [S4], and for completeness, we explain the main principles here. We denote $\rho(t)$ the density operator of the transmon-resonator system. This system's dynamics are driven by the time dependent Hamiltonian $\boldsymbol{H}(t)$ of Eq. (1) in the main text, and by a coupling to

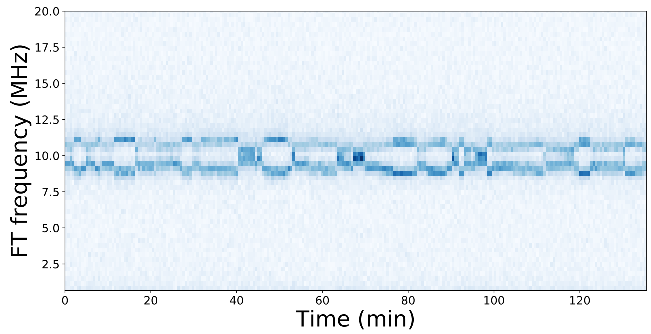

FIG. S3. Fourier transform (FT) of the Ramsey signal of the $|g\rangle$ to $|e_6\rangle$ transition, measured repeatedly every 32 seconds over a period of about 2 hours. Due to quasiparticle tunneling, two frequencies appear in each Ramsey signal. These frequencies drift over a timescale of several minutes due to background charge motion [S3].

a bath through an operator $\boldsymbol{X}$. Typically, $\boldsymbol{X} = \boldsymbol{a} + \boldsymbol{a}^\dagger$, and the bath is a transmission line. For simplicity, we neglect the direct coupling of the transmon to the bath, but this can easily be included in the theory by changing $\boldsymbol{X}$. We recall that $\boldsymbol{H}(t)$ is periodic with period $T_p = 2\pi/\omega_p$, where ω_p is the pump frequency. The goal is to find $\rho(t)$ in the infinite time limit.

After a sufficiently long time, $\rho(t)$ reaches a limit-cycle: a T_p-periodic trajectory denoted $\bar{\rho}(t)$. We find this limit-cycle using Floquet-Markov theory [S5]. This theory assumes a weak coupling to the bath, but can treat pumps of arbitrary amplitudes and frequencies.

Change of frame: The first step is to write the Hamiltonian in a frame where the resonator is close to the vacuum state. We do this by solving the quantum Langevin equations when $E_J = 0$. We will use the following useful formulas [S6, (4.12)]:

$$[\boldsymbol{\theta}, \boldsymbol{N}] = i \ ,$$

and hence for any analytic function f

$$[\boldsymbol{\theta}, f(\boldsymbol{N})] = i\frac{\partial f}{\partial \boldsymbol{N}}(\boldsymbol{N}) \ ,$$

and also

$$[\boldsymbol{a}, f(\boldsymbol{a}^\dagger)] = \frac{\partial f}{\partial \boldsymbol{a}^\dagger}(\boldsymbol{a}^\dagger) \ .$$

We denote $\boldsymbol{a}_0, \boldsymbol{N}_0, \boldsymbol{\theta}_0$ the solutions of the Langevin equations associated to Hamiltonian (1) of the main text with $E_J = 0$. We find:

$$\begin{aligned}
\frac{d}{dt}\boldsymbol{a}_0 &= \frac{1}{i\hbar}[\boldsymbol{a}_0, \boldsymbol{H}] = -i\omega_0\boldsymbol{a}_0 - ig\boldsymbol{N}_0 - i\mathcal{A}_p(t) \\
\frac{d}{dt}\boldsymbol{N}_0 &= \frac{1}{i\hbar}[\boldsymbol{N}_0, \boldsymbol{H}] = 0 \\
\frac{d}{dt}\boldsymbol{\theta}_0 &= \frac{1}{i\hbar}[\boldsymbol{\theta}_0, \boldsymbol{H}] = 8E_C/\hbar\boldsymbol{N}_0 + g(\boldsymbol{a}_0 + \boldsymbol{a}_0^\dagger) \ ,
\end{aligned}$$

where $\mathscr{A}_p(t) = A_p \cos(\omega_p t)$, and $A_p \geq 0$. These equations are linear, and are therefore easy to solve. We introduce the expectation values: $\langle \boldsymbol{a}_0 \rangle = a_0, \langle \boldsymbol{N}_0 \rangle = N_0, \langle \boldsymbol{\theta}_0 \rangle = \theta_0$. Using some approximations [S4], we find

$$\begin{aligned} a_0(t) &= \frac{A_p/2}{(\omega_p - \omega_a)} e^{-i\omega_p t} \\ N_0(t) &= 0 \\ \theta_0(t) &= g \frac{A_p}{\omega_p(\omega_p - \omega_a)} \sin(\omega_p t) \ . \end{aligned}$$

We define

$$\bar{n} = \left| \frac{A_p/2}{\omega_p - \omega_a} \right|^2 \ . \tag{S7}$$

For simplicity we assume $\omega_p > \omega_a$. If $\omega_p < \omega_a$ then one needs to multiply the following solutions by -1. We get

$$\begin{aligned} a_0(t) &= \sqrt{\bar{n}} e^{-i\omega_p t} \\ N_0(t) &= 0 \\ \theta_0(t) &= 2 \frac{g}{\omega_p} \sqrt{\bar{n}} \sin(\omega_p t) \ . \end{aligned} \tag{S8}$$

Comparing Eq. (S7), and Eq. (S4), we see that the expressions of $\bar{n}$ and $\bar{n}_r$ are very similar, and differ only by the presence of subscripts r, and the term in κ_r in Eq. (S4). In the limit of large detunings: $|\omega_r - \omega_p| \gg \kappa_r$, and hence the term in κ_r can be neglected. The pump amplitude $A_{p,r}$ slightly differs from A_p due to the transmon-resonator mode hybridization. For our experimental parameters, $A_{p,r}$ and A_p differ by less than 1%. The measured resonator frequency ω_r roughly varies between $\bar{\omega}_r$ and ω_a, spanning about 20 MHz. For the simulation of Fig. 1b of the main text, we consider a pump at frequency $\omega_p/2\pi = 8.1$ GHz, which is detuned from the resonator by about 340 MHz. This detuning is much larger than the frequency variation of ω_r. Hence $\bar{n}$ and $\bar{n}_r$ differ by less than 15%.

We now move to a frame around the solutions given in Eq. (S8), introducing $\tilde{\boldsymbol{\theta}} = \boldsymbol{\theta} - \theta_0$, $\tilde{\boldsymbol{N}} = \boldsymbol{N} - N_0$ and $\tilde{\boldsymbol{a}} = \boldsymbol{a} - a_0$. This frame is chosen such that the deviation of the resonator from the vacuum is small, and hence we can use a low truncation for the resonator mode. This change of frame leads to the following Hamiltonian [S4]:

$$\begin{aligned} \tilde{\boldsymbol{H}} &= 4E_C \tilde{\boldsymbol{N}}^2 - E_J \cos\left(\tilde{\boldsymbol{\theta}} + \theta_0(t)\right) \\ &\quad + \hbar\omega_a \tilde{\boldsymbol{a}}^\dagger \tilde{\boldsymbol{a}} + \hbar g \tilde{\boldsymbol{N}} \left(\tilde{\boldsymbol{a}} + \tilde{\boldsymbol{a}}^\dagger\right) \\ &= 4E_C \tilde{\boldsymbol{N}}^2 - E_J \left(\cos(\tilde{\boldsymbol{\theta}}) \cos(\theta_0(t)) - \sin(\tilde{\boldsymbol{\theta}}) \sin(\theta_0(t))\right) \\ &\quad + \hbar\omega_a \tilde{\boldsymbol{a}}^\dagger \tilde{\boldsymbol{a}} + \hbar g \tilde{\boldsymbol{N}} \left(\tilde{\boldsymbol{a}} + \tilde{\boldsymbol{a}}^\dagger\right) \end{aligned}$$

We write $\tilde{\boldsymbol{H}}$ as a matrix in the basis spanned by $|T_k\rangle \otimes |F_l\rangle$, where $|T_k\rangle$ are eigenstates of the transmon Hamitlonian $4E_C\tilde{\boldsymbol{N}}^2 - E_J \cos\left(\tilde{\boldsymbol{\theta}}\right)$, and $|F_l\rangle$ are Fock states: eigenstates of the resonator Hamiltonian $\hbar\omega_a \tilde{\boldsymbol{a}}^\dagger \tilde{\boldsymbol{a}}$. We truncate this basis to $M = 450$ states, with 45 states for the transmon and 10 states for the resonator.

Floquet analysis: Using functions provided by the Quantum Toolbox in Python (Qutip), we compute the Floquet states of $\tilde{\boldsymbol{H}}(t)$, which we denote $|\psi_\alpha(t)\rangle$ for $\alpha = 1, \ldots, M$. We can then calculate the dissipation operator $\boldsymbol{X}$ matrix elements in the Floquet basis $|\psi_\alpha\rangle$ [S25, (245)].

With these matrix elements, we can now calculate the master equation followed by the density matrix [S25, (251)], and compute its steady state in the Floquet basis: $\bar{\rho}(t) = \sum_\alpha \rho_{\alpha\alpha} |\psi_\alpha(t)\rangle \langle\psi_\alpha(t)|$. We recall that $\bar{\rho}(t)$ is T_p-periodic and we define $\bar{\rho}_0 = \bar{\rho}(0)$. We can express $\bar{\rho}_0$ in the basis $\{|T_k\rangle \otimes |F_l\rangle\}_{k,l}$, and calculate the partial trace with respect to the cavity $\bar{\rho}_{0q} = \mathrm{Tr}_{\mathrm{cav}}(\bar{\rho}_0) = \sum_l \langle F_l| \bar{\rho}_0 |F_l\rangle$. The diagonal of $\bar{\rho}_{0q}$: $\mathrm{diag}(\bar{\rho}_{0q})$ is the list of the transmon eigenstate populations. Note that at times $t_m = 0 + mT_p$, $\theta_0(t_m) = 0$, hence the unitary which transforms states between the displaced frame back to the original one is the identity for the transmon degree of freedom. In Fig. 1c of the main text, we plot $\mathrm{diag}(\bar{\rho}_{0q})$ as a function of $\bar{n}$, where $\bar{n}$ given in Eq. (S7).

QUASIPARTICLE GENERATION

In the main text, we discuss whether the strong pump we apply on the system generates quasiparticles. If the pump significantly increases the quasiparticle density, the transmon T_1 will decrease [S7, S8]. In Fig. S4a, we reproduce the experiment of Fig. 3b in the main text for various pump powers, which correspond to various numbers of photons $\bar{n}_r$. For small $\bar{n}_r$, the transmon is not excited, while for large $\bar{n}_r$, the transmon is driven to highly excited states. Additionally, after each pump pulse, we measure the transmon T_1 after a time delay chosen so that all modes have decayed back to their ground state. We find no decrease in T_1 (Fig. S4b) which means that the pump can expel the transmon out of its potential well without producing a measurable amount of quasiparticles.

* raphael.lescanne@lpa.ens.fr
† zaki.leghtas@mines-paristech.fr

[S1] Q. Ficheux, S. Jezouin, Z. Leghtas, and B. Huard, Nature Communications, in press (2018).
[S2] J. Gambetta, A. Blais, D. I. Schuster, A. Wallraff, L. Frunzio, J. Majer, M. H. Devoret, S. M. Girvin, and R. J. Schoelkopf, Phys. Rev. A **74**, 042318 (2006).
[S3] D. Ristè, C. C. Bultink, M. J. Tiggelman, R. N. Schouten, K. W. Lehnert, and L. DiCarlo, Nature Communications **4**, 1913 EP (2013).
[S4] L. Verney, R. Lescanne, J. Venkatraman, W. C. Smith, , M. H. Devoret, Z. Leghtas, and M. Mirrahimi, In preparation (2018).
[S5] M. Grifoni and P. Hänggi, Physics Reports **304**, 229 (1998).

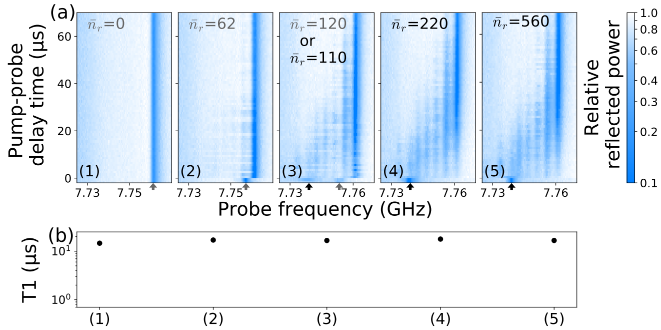

FIG. S4. Transmon relaxation following a pump pulse of increasing power. (**a**) Same experiment as in Fig. 3b in the main text for increasing pump power from a1 to a5, a5 corresponding to the maximum power the microwave source could deliver. (**a1**-**a2**) The pump induces an AC Stark shift proportional to $\bar{n}_r$ at $t < 0$ but does not significantly excite the transmon. (**a3**) At intermediate pump powers, the system is in a statistical mixture of two configurations, as indicated by the two dips at $t < 0$. One corresponds to the AC Stark shifted cavity, the other to the bare cavity frequency ω indicating that the transmon gets highly excited. (**a4**-**a5**) At higher pump powers, the cavity frequency always jumps to ω and the transmon decays as in Fig. 3b in the main text. (**b**) Transmon T_1 (y-axis) measured 50 μs after a pump is applied. The pump duration and powers (x-axis) correspond to the ones used for the experiments shown in (a). T_1 does not decrease as the pump power increases which indicates that the pump does not generate a measurable increase in the quasiparticle density [S7, S8].

[S6] M. H. Devoret, Les Houches Session LXIII, Quantum Fluctuations , 351 (1995).

[S7] C. Wang, Y. Y. Gao, I. M. Pop, U. Vool, C. Axline, T. Brecht, R. W. Heeres, L. Frunzio, M. H. Devoret, G. Catelani, L. I. Glazman, and R. J. Schoelkopf, Nature Communications **5**, 5836 EP (2014).

[S8] U. Vool, I. M. Pop, K. Sliwa, B. Abdo, C. Wang, T. Brecht, Y. Y. Gao, S. Shankar, M. Hatridge, G. Catelani, M. Mirrahimi, L. Frunzio, R. J. Schoelkopf, L. I. Glazman, and M. H. Devoret, Phys. Rev. Lett. **113**, 247001 (2014).